Pergamon

Int. J. Heat Mass Transfer. Vol. 37, No. 13, pp. 1957–1968, 1994

0017-9310/94 $7.00 + 0.00

0017-9310(94)E0052-V

The daytime circulation and temperature structure in a reservoir sidearm

D. E. FARROW† and J. C. PATTERSON

Centre for Water Research, University of Western Australia, Nedlands, Western Australia 6009

(*Received* 20 *July* 1992)

Abstract—During the daylight hours, the shallow regions of a reservoir sidearm absorb more heat per unit volume than the deeper parts, leading to a nett horizontal pressure gradient that drives a circulation in the sidearm. The spin up time for a typical sidearm is of the order of or longer than a day, implying that the flow is intrinsically unsteady. In this paper, the unsteady daytime circulation and temperature structure in a reservoir sidearm is modelled by the natural convection of a fluid contained in a 2-D, triangular cavity. The absorption of solar radiation that drives the flow is modelled by Beer's law and a heat flux bottom boundary condition formulated from the amount of heat that penetrates the entire local depth. Asymptotic solutions of the resulting equations are found and these reproduce some of the observed features of the daytime circulation in a reservoir sidearm.

1. INTRODUCTION

THE UNDERSTANDING of the fluid mechanics of lakes and reservoirs has expanded rapidly in recent years owing to the importance of fluid dynamical processes for determining the quality of water supply. A recent review of dynamical processes pertinent to lakes and reservoirs can be found in Imberger and Patterson [1]. In particular, processes that give rise to horizontal rather than vertical transport of water properties have received considerable recent attention. An example of a limnological situation where horizontal processes play a part in the overall dynamics is differential heating or cooling, which occurs when neighboring regions of the same water body are heated or cooled relative to each other. This leads to a horizontal pressure gradient due to thermal expansion and a significant flow may result. The flooding of a reservoir basin usually involves the inundation of many small valleys around its perimeter. These flooded valleys (which are then called sidearms) are typically only tens to hundreds of metres long and only a few metres deep where they join with the main body of the reservoir. Sidearms are often well protected from the wind and so thermal forcing associated with differential heating and cooling is an important mechanism for promoting exchange of water between the sidearm and the main body of the reservoir.

During the day, the water column absorbs solar radiation according to Beer's law [2]; the intensity of the light decays exponentially with depth and the rate of decay is a function of the wavelength of the light and the turbidity of the water. This leads to a shallow surface layer that can be several degrees warmer than the underlying water. Near the shore, topographic effects become important as the heat absorbed is distributed over a decreasing depth and the water in the shallows becomes, on average, warmer than the deeper offshore regions. As pointed out by Monismith *et al.* [3], this heating mechanism leads to the temperature scaling with the inverse of the distance from the shore. This temperature structure drives a surface outflow of warm water from the edges of a reservoir sidearm. Flows due to this mechanism have been observed by Adams and Wells [4] and Monismith *et al.* [3] with measured velocities of the order of 5 cm s^{-1}. These studies also indicated that the three-dimensional topography of a reservoir sidearm may lead to a complicated three-dimensional velocity and temperature structure.

In the absence of wind or other momentum inputs, the flow described above can be classified as natural convection, for which there is a large body of literature. Natural convection in shallow cavities is the most relevant to the geophysical phenomena considered in this paper.

Sturm [5] and Jain [6] studied a cooling pond sidearm and their studies are relevant to the present situation. In those papers, steady-state integral solutions for heat and mass fluxes in idealized cooling pond sidearms were found which are consistent with the experimental results of Brocard and Harleman [7]. Poulikakos and Bejan [8] found the steady-state flow and temperature structure in an attic space with a horizontal bottom and an arbitrarily shaped heated

†Present address: School of Mathematics, University of East Anglia, Norwich NR4 7TJ, U.K.

NOMENCLATURE

A bottom slope
$a_n, b_n, c_n, n = 0, 1, \ldots$ coefficients
C_p specific heat of water
$F_{4nm}, \ldots, F_{6nm}$ special functions
g acceleration due to gravity
Gr Grashof number, $Gr = g\alpha I_0/(\rho_0 C_p \kappa^3 \eta^4)$
H_0 surface heating intensity [°C m^{-2} s^{-1}]
h vertical length scale
I radiation intensity [W m^{-2}]
I_0 intensity of radiation incident on the surface [W m^{-2}]
l horizontal length-scale
p' pressure
Q internal temperature source [°C s^{-1}]
Q_0 magnitude of internal temperature source
t' time
t non-dimensional time, $t = t'\kappa\eta^2$
t_e e-folding time
T' temperature
T non-dimensional temperature $T = (T' - T_0)\rho_0 C_p \kappa\eta/I_0$
T_0 reference temperature
$T^{(0)}$ asymptotic temperature solution
u', w' velocities
u, w non-dimensional velocities $u = u'/(A\ Gr\ \kappa\eta)$ and $w = w'/(A^2\ Gr\ \kappa\eta)$
x', z' Cartesian coordinate system, z vertical
x, z non-dimensional coordinate system, $x = A\eta x'$ and $z = \eta z'$.

Greek symbols
α thermal expansion coefficient
β_n eigenvalues
ΔT temperature range-scale
η attenuation coefficient [m^{-1}]
κ thermal diffusivity
ν kinematic viscosity
ρ_0 reference density
σ Prandtl number, ν/κ
ψ non-dimensional streamfunction
$\psi^{(0)}$ asymptotic streamfunction solution
$\psi_1^{(0)}, \ldots, \psi_3^{(0)}$ parts of asymptotic streamfunction solution
$\psi_{4n}^{(0)}, \ldots, \psi_{6n}^{(0)}$ parts of asymptotic streamfunction solution.

Subscripts
$(.)_x$, etc. partial differentiation.

Superscripts
$(.)^{(k)}, k = 0, 2, \ldots$ terms in asymptotic expansion.

upper boundary using asymptotic methods. In more directly geophysically motivated studies, Scott and Imberger [9] and Scott [10] considered the steady-state flow in three-dimensional cavities of arbitrary geometry which were used to model estuarine dynamics. Those studies considered the steady-state density and flow structures in two- and three-dimensional estuaries which are subject to a number of buoyancy and momentum inputs, again using asymptotic methods.

All of this work has been for steady-state conditions. However, Monismith *et al.* [3] show that the spin-up time for a typical sidearm is at least of the same order as the period of the diurnal forcing which means that during the day, at least in the deeper parts of a sidearm, steady state is not achieved before there is a change in the nature of the forcing. This was confirmed by the observations of Monismith *et al.* where the night-time flow in the sidearm did not reverse until about 7 h after the heat flux at the surface had changed from cooling to heating. Consequently, the flow is intrinsically unsteady and the transient behavior must also be included in a model of sidearm behavior.

Patterson [11] studied transient natural convection in an internally heated rectangular cavity which was initially isothermal and at rest. He found that the approach to steady state could be classified as either conductive, transitional or convective, depending on the value of the Grashof number, Gr, relative to various combinations of the aspect ratio of the cavity and the Prandtl number $\sigma = \nu/\kappa$ of the fluid, where:

$$Gr = \frac{g\alpha\Delta T h^3}{\nu^2}. \tag{1}$$

In equation (1) and the definition of σ, g is the acceleration due to gravity, α is the thermal expansion coefficient, $\Delta T = Q_0 h l^3/\nu$, where Q_0 °C m^{-2} s^{-1} is the magnitude of the volumetric heating rate, l is the length of the cavity, h is the height of the cavity, ν is the kinematic viscosity and κ is the thermal diffusivity [11]. The classifications could be further divided into subclassifications characterized by the relative magnitudes of various time-scales of the flow and the nature of the internal balances at steady state. In some cases, the approach to steady state was oscillatory, but in all cases it was achieved in a time scale of h^2/ν, which is a scale for the time it takes for viscosity to diffuse momentum across the depth of the cavity. For

a reservoir sidearm, h is typically 5 m, leading to a spin-up time of $\sim 2.5 \times 10^7$ s (≈ 250 days) for molecular viscosity or $\sim 2.5 \times 10^5$ s (≈ 2.5 days) for a typical value of the eddy viscosity of 10^{-4} m^2 s^{-1} [4]. Thus, even if the flow is turbulent, the spin-up time is comparable to the time scale of the forcing and so, as already discussed, the flow in a typical sidearm is intrinsically unsteady.

There are very few analytical or experimental studies aimed at understanding the transient response of a cavity with sidearm geometry to thermal forcing. Patterson [12] numerically investigated the daytime circulation, assuming that the heat input was uniformly distributed over the local depth in a triangular cavity. Further assuming that the bottom of the model sidearm was perfectly reflective and the bottom slope was small led to a horizontally linear internal heating source term. An additional feature of this model was an adjustment of the mean heat input so the system would reach steady state. The results of Patterson [12] show that, even though the internal heating is vertically uniform, advection ultimately sets up a strong stratification with horizontal isotherms in the majority of the cavity and vertical isotherms occurring only in the shallow tip region.

There appear to be no analytical or experimental studies of unsteady natural convection forced by the absorption of solar radiation in sidearm geometries. Asymptotic solutions for the diurnally forced case, including the effects of unsteady forcing, have been found by Farrow and Patterson [13]. Inherent in that work is the simplifying assumption that the heat input and output is vertically uniform and thus, to first order, the resulting temperature structure is also vertically uniform. The current work is concerned with the daytime forcing only, with radiation absorption following Beer's law, potentially leading to a strong temperature stratification.

2. MODEL FORMULATION

The daytime flow within the sidearm is modelled by the flow of a fluid contained in the wedge $-Ax' < z' < 0$ in the (x', z') plane where A is the bottom slope of this idealised sidearm (see Fig. 1). This is the simplest domain that allows for a continuously variable depth [13]. The equations governing the flow and temperature within the sidearm are:

$$\frac{\partial u'}{\partial t'} + u'\frac{\partial u'}{\partial x'} + w'\frac{\partial u'}{\partial z'} = -\frac{1}{\rho_0}\frac{\partial p'}{\partial x'} + \nu\nabla^2 u', \quad (2)$$

$$\frac{\partial w'}{\partial t'} + u'\frac{\partial w'}{\partial x'} + w'\frac{\partial w'}{\partial z'} = -\frac{1}{\rho_0}\frac{\partial p'}{\partial z'} + \nu\nabla^2 w' + g\alpha(T' - T_0), \quad (3)$$

$$\frac{\partial T'}{\partial t'} + u'\frac{\partial T'}{\partial x'} + w'\frac{\partial T'}{\partial z'} = \kappa\nabla^2 T' + Q(x', z', t'), \quad (4)$$

$$\frac{\partial u'}{\partial x'} + \frac{\partial w'}{\partial z'} = 0. \quad (5)$$

The form of the internal heating term Q is chosen to reflect the daytime heating cycle of a reservoir sidearm. During the day, the water in a sidearm absorbs solar radiation incident on the surface. The radiation intensity at a particular wavelength decreases with depth according to Beer's law [14]:

$$I = I_0 e^{\eta z'} \text{ W m}^{-2} \quad (6)$$

where I_0 is the intensity at the surface and η is the attenuation coefficient which is a function of the wavelength of the incident radiation and the turbidity of the water. For the purposes of this model, it is assumed that the radiation is characterized by a single wavelength and the water has a uniform turbidity and thus a single and constant attenuation coefficient. Solar radiation is often characterized by a few discrete wavelengths with various intensities and attenuation coefficients associated with each one [14]. Later in this paper, the problem is linearized and so the solutions associated with any extra wavelengths could be superimposed to more accurately represent any particular radiation. Assuming no reflection, the corresponding volumetric heating rate is given by:

$$Q = \frac{I_0}{\rho_0 C_p}\eta e^{\eta z'} \equiv H_0 \eta e^{\eta z'} \text{ C s}^{-1}, \quad (7)$$

where C_p is the specific heat of water at constant

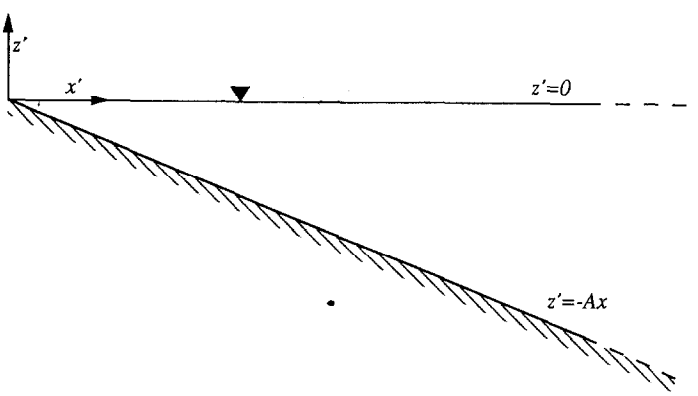

FIG. 1. Schematic of the flow domain showing the geometry and coordinate system.

pressure and $H_0 = I_0/(\rho_0 C_p)$. This is the assumed form for Q for the daytime circulation used in equation (4).

The internal heating Q defined by equation (7) is horizontally uniform and so in itself will not generate a horizontal pressure gradient to drive a flow in the sidearm. The principal driving mechanism for the circulation comes from the temperature boundary condition applied at the sloping bottom boundary $z' = -Ax'$. Clearly, there will be some radiation that penetrates all the way to the bottom of the sidearm. For this model, it is assumed that this radiation is absorbed by the bottom which then immediately releases this heat as a bottom boundary heat flux. This leads to a boundary condition for the temperature:

$$\frac{\partial T'}{\partial \hat{n}} = \frac{1}{\sqrt{1+A^2}}\left(A\frac{\partial T'}{\partial x'} + \frac{\partial T'}{\partial z'}\right) = -\frac{1}{\kappa} H_0 e^{-A\eta x'} \quad \text{on} \quad z' = -Ax', \tag{8}$$

where $\hat{n}$ is the direction normal to the sloping bottom. This boundary condition yields a temperature with a strong horizontal dependence, especially near the tip $x' = 0$ where topographic effects are important.

At the upper boundary, it is assumed here that during the day the amount of heat transferred through the surface by sensible heat transfer, evaporation or long-wave radiation is small compared with the amount absorbed via solar radiation. In other words, it is assumed here that the surface is insulated so that:

$$\frac{\partial T'}{\partial z'} = 0 \quad \text{on} \quad z' = 0. \tag{9}$$

The natural velocity boundary conditions that most realistically (in the absence of any wind) model a sidearm are that the bottom is solid and that the surface is stress free, that is:

$$\frac{\partial u'}{\partial z'} = w' = 0 \quad \text{on} \quad z' = 0, \tag{10}$$

$$u' = w' = 0 \quad \text{on} \quad z' = -Ax'. \tag{11}$$

It now only remains to define the far field ($x \to \infty$) and initial conditions for this model. The initial conditions are that the fluid in the sidearm is initially at rest and has a uniform temperature. That is:

$$u' = w' = 0, \quad T' = T_0 \quad \text{at} \quad t' = 0. \tag{12}$$

In a real sidearm, there may be some structure associated with the previous night's cooling but, in this idealized model, the primary interest is in the spin up of the daytime flow: thus the simple initial conditions (12) are used. In the solution method adopted in this paper, far field conditions are not necessary: however, for completeness, they are ψ, $T_x \to 0$ as $x \to \infty$.

Equations (2)–(5) along with the boundary and initial conditions (8)–(12) and the far field conditions fully define an idealized, two-dimensional model for the daytime circulation in a reservoir sidearm. The system of equations is non-linear and there is no general method available for finding the solution. However asymptotic solutions for the unsteady temperature and velocity fields can be obtained.

The system of equations (2)–(12) is non-dimensionalized in the following way. Since the geometry of the cavity imposes no natural length-scale, the only length-scale available is the inverse of the attenuation coefficient η. Thus, the vertical coordinate must scale like $z' \approx \eta^{-1}$. The geometry of the cavity then provides a scale for the horizontal coordinate, $x' \approx (A\eta)^{-1}$. The flow is driven by the generation of a temperature gradient which suggests that the temperature diffusion scale is the appropriate time-scale, that is $t' \sim (\kappa\eta^2)^{-1}$. The remaining scales are obtained by first balancing the unsteady term in the temperature equation (4) against the source term to give a scale for $T' - T_0 = \Delta T \approx H_0(\kappa\eta)$. Assuming that the flow is close to hydrostatic yields a scale for the horizontal velocity $u' \approx A\,Gr\,\kappa\eta$ where the Grashof number Gr for this paper is given by:

$$Gr = \frac{g\alpha H_0}{\kappa^3 \eta^4}. \tag{13}$$

Finally, the continuity equation (5) gives a scale for the vertical velocity $w' \approx A^2\,Gr\,\kappa\eta$. Using these scales to nondimensionalize equations (2)–(12), eliminating the pressure and introducing a non-dimensional stream function ψ, where the dimensionless velocities are $u = -\psi_z$ and $w = \psi_x$, yields the equations:

$$\psi_{tzz} + A^2\psi_{txx} + A^2\,Gr(\psi_x\psi_{zzz} - \psi_z\psi_{zzx}) + A^4\,Gr(\psi_x\psi_{xxz} - \psi_z\psi_{xxx}) = \sigma(\psi_{zzzz} + 2A^2\psi_{xxzz} + A^4\psi_{xxxx}) + T_x, \tag{14}$$

and

$$T_t + A^2\,Gr(-\psi_z T_x + \psi_x T_z) = A^2 T_{xx} + T_{zz} + e^z, \tag{15}$$

where all variables are now dimensionless. The boundary conditions become:

$$\psi = \psi_{zz} = 0, \quad T_z = 0 \quad \text{on} \quad z = 0, \tag{16}$$

$$\psi = \psi_z = 0, \quad \frac{T_z + A^2 T_x}{\sqrt{1+A^2}} = -e^{-x} \quad \text{on} \quad z = -x, \tag{17}$$

and the initial conditions $T = \psi = 0$ at $t = 0$.

3. ASYMPTOTIC SOLUTION

The small parameter A appears as even powers in the above boundary value problem. Following Cormack *et al.* [15], the dependent variables are expanded as a series in A^2:

$$T = T^{(0)} + A^2 T^{(2)} + A^4 T^{(4)} + \ldots$$
$$\psi = \psi^{(0)} + A^2\psi^{(2)} + A^4\psi^{(4)} + \ldots. \tag{18}$$

Substituting these expressions in equations (14) and

(15) and equating like powers of A yields a system of equations that can, in principle, be solved recursively. The general $O(A^n)$ equations are (n even):

$$\psi_{tzz}^{(n)}+\psi_{txx}^{(n-2)}+Gr\sum_{\substack{k=0\\k\text{ even}}}^{n-2}[\psi_x^{(k)}\psi_{zzz}^{(n-k-2)}-\psi_z^{(k)}\psi_{zzx}^{(n-k-2)}]$$

$$+Gr\sum_{\substack{k=0\\k\text{ even}}}^{n-4}[\psi_x^{(k)}\psi_{xxz}^{(n-k-4)}-\psi_z^{(k)}\psi_{xxx}^{(n-k-4)}]$$

$$=\sigma(\psi_{zzzz}^{(n)}+2\psi_{xxzz}^{(n-2)}+\psi_{xxxx}^{(n-4)})+T_x^{(n)} \quad (19)$$

and:

$$T_t^{(n)}+Gr\sum_{\substack{k=0\\k\text{ even}}}^{n-2}[-\psi_z^{(k)}T_x^{(n-k-2)}+\psi_x^{(k)}T_z^{(n-k-2)}]$$

$$=T_{zz}^{(n)}+T_{xx}^{(n-2)}+\delta_{n0}e^z, \quad (20)$$

with surface boundary conditions:

$$\psi^{(n)}=\psi_{zz}^{(n)}=0 \quad \text{on} \quad z=0$$

$$T_z^{(n)}=0 \quad \text{on} \quad z=0, \quad (21)$$

and bottom boundary conditions:

$$\psi^{(n)}=\psi_z^{(n)}=0 \quad \text{on} \quad z=-x,$$

$$T_z^{(n)}+\sum_{\substack{k=2\\k\text{ even}}}^{n-2}(-1)^{k/2}\frac{1.3\ldots(k-1)}{2.4\ldots k}(T_z^{(n-k)}+T_x^{(n-k-2)})$$

$$=-\delta_{n0}e^{-x} \quad \text{on} \quad z=-x, \quad (22)$$

where quantities with negative superscripts are zero and $\delta_{n0}=1$ if $n=0$ and is zero otherwise. Only the $O(A^0)$ equations are solved here. These equations are:

$$\psi_{tzz}^{(0)}=\sigma\psi_{zzzz}^{(0)}+T_x^{(0)}, \quad (23)$$

$$T_t^{(0)}=T_{zz}^{(0)}+e^z, \quad (24)$$

with boundary conditions:

$$\psi^{(0)}=\psi_{zz}^{(0)}=T_z^{(0)}=0 \quad \text{on} \quad z=0$$

$$\psi^{(0)}=\psi_z^{(0)}=0, \quad T_z^{(0)}=-e^{-x} \quad \text{on} \quad z=-x, \quad (25)$$

and the initial conditions $\psi^{(0)}=T^{(0)}=0$ at $t=0$. The equations for $\psi^{(0)}$ and $T^{(0)}$ are linear and algebraic in the horizontal coordinate, greatly simplifying the analysis. These equations show that at zero order in A, the only processes that are significant are for $T^{(0)}$, vertical conduction and internal heating and for $\psi^{(0)}$, vertical shear and buoyancy.

The zero-order temperature is a standard unsteady, one-dimensional heat conduction problem. There is a slight difficulty in that the system does not have a steady state since heat is continuously added but none is allowed to escape either through the boundaries or horizontally. The solution can be found by taking Laplace transforms in t and is given by:

$$T^{(0)}=\frac{t}{x}-e^z+\frac{z^2}{2x}+z+\frac{1}{3}x+\frac{1}{x}(1-e^{-x})$$

$$-\frac{2}{x}\sum_{n=1}^{\infty}\left[\frac{1}{(n\pi/x)^2}-\frac{1-(-1)^ne^{-x}}{1+(n\pi/x)^2}\right]$$

$$\times\exp\left[-\left(\frac{n\pi}{x}\right)^2t\right]\cos\left(\frac{n\pi}{x}z\right). \quad (26)$$

It should be stressed that this temperature solution does not include the effects of convection or horizontal conduction which are both second-order effects and would thus appear in $T^{(2)}$.

The forcing term in equation (23) is given by:

$$T_x^{(0)}=a_0(x)+b_0(x)z^2+c_0(x)t$$

$$+\sum_{n=1}^{\infty}a_n(x)e^{-(n\pi/x)^2t}\cos(n\pi z/x)$$

$$+\sum_{n=1}^{\infty}b_n(x)te^{-(n\pi/x)^2t}\cos(n\pi z/x)$$

$$+\sum_{n=1}^{\infty}c_n(x)ze^{-(n\pi/x)^2t}\sin(n\pi z/x), \quad (27)$$

where a_n, b_n and c_n, $n=0,1,2,\ldots$, are given for $n=0$ by:

$$a_0=\frac{1}{3}-\frac{1}{x^2}(1-e^{-x})+\frac{1}{x}e^{-x}$$

$$b_0=-\frac{1}{2x^2}$$

$$c_0=-\frac{1}{x^2}, \quad (28)$$

and for $n=1,2,\ldots$:

$$a_n=\frac{2}{x^2}\left[\frac{1}{(n\pi/x)^2}-\frac{1-(-1)^ne^{-x}}{1+(n\pi/x)^2}\right]-\frac{2}{x}\left\{\frac{2x}{(n\pi)^2}\right.$$

$$\left.-\frac{(-1)^ne^{-x}[1+(n\pi/x)^2]+2(n\pi)^2[1-(-1)^ne^{-x}]/x^3}{[1+(n\pi/x)^2]^2}\right\}$$

$$b_n=-\frac{4}{x^2}\left[\frac{1}{(n\pi/x)^2}-\frac{1-(-1)^ne^{-x}}{1+(n\pi/x)^2}\right]$$

$$c_n=-\frac{2n\pi}{x^3}\left[\frac{1}{(n\pi/x)^2}-\frac{1-(-1)^ne^{-x}}{1+(n\pi/x)^2}\right]. \quad (29)$$

At this point, it is interesting to note how each part of the forcing term arises. The a_0+c_0t terms are independent of z and represent the mean horizontal gradient of $T^{(0)}$. All terms except the c_0t term remain finite or vanish as t becomes large. Thus, as $t\to\infty$, the c_0t term will dominate and the temperature will be vertically uniform. This means that at large times the zero-order flow will not be affected by any vertical structure in the temperature. The b_0z^2 term represents a change in the horizontal temperature gradient with

depth. This arises because the isotherms in the flow domain must curl over to meet the boundary condition at $z = -x$. The remaining terms arise from the transient terms of $T^{(0)}$. Notable for its absence is that part of $T^{(0)}$ (namely e^z) which balances the internal heating. That part of the solution has no horizontal dependence and thus has no effect on the flow at zero order.

The boundary value problem for $\psi^{(0)}$ is linear and so each term of the forcing function $T_x^{(0)}$ can be considered separately and then the corresponding solutions superimposed. The solution can be found using Laplace transforms in t: however, the details are tedious and are not included here. The full solution for $\psi^{(0)}$ is given by:

$$\psi^{(0)} = a_0\psi_1^{(0)} + b_0\psi_2^{(0)} + c_0\psi_3^{(0)} + \sum_{n=1}^{\infty} (a_n\psi_{4n}^{(0)} + b_n\psi_{5n}^{(0)} + c_n\psi_{6n}^{(0)}), \quad (30)$$

where $\psi_1^{(0)}$, $\psi_2^{(0)}$, $\psi_3^{(0)}$, $\psi_{4n}^{(0)}$, $\psi_{5n}^{(0)}$, and $\psi_{6n}^{(0)}$ are given in the Appendix and a_n, b_n and c_n, $n = 0, 1, 2, \ldots$, are given by equations (28) and (29).

4. DISCUSSION

4.1. *Preliminary remarks*

It is important to note from the outset that the asymptotic solutions found above for the daytime circulation have no steady state. This fact manifests itself via the continuously increasing temperature. Also, there is a continuously increasing horizontal temperature gradient which implies that the velocities in the model sidearm also never reach a steady state. However, the system does ultimately reach a quasi-steady state. Both $T^{(0)}$ and $\psi^{(0)}$ include terms that are proportional to t which dominate for large times. For $T^{(0)}$, the large time behavior is $T^{(0)} \to t/x$ as $t \to \infty$ which is a vertically uniform temperature with an ever increasing horizontal gradient. This in turn leads to an ever increasing magnitude of the circulation in the sidearm with the large time behavior of $\psi^{(0)}$ being:

$$\psi^{(0)} \to -\frac{t}{48\sigma x^2} z(z+x)^2(2z-x) \quad \text{as} \quad t \to \infty. \quad (31)$$

The above large time behavior of $\psi^{(0)}$ is the same (up to a variable transform and the time dependence) as the steady-state solution found by Cormack *et al.* [16] for the flow in a rectangular cavity with differentially heated end walls and a stress free surface. The lack of a steady-state solution is of no great concern since in this paper the primary interest is in the transient response. In a real sidearm, the solutions here will only be of interest while the daytime forcing is applied and the accelerating flow will eventually be countered by the reverse pressure gradient established by nighttime cooling. Thus these results describe only the spin up of the daytime circulation.

Even though the behavior above has been dubbed the large time behavior, this is not strictly correct. The e-folding times of the transient terms of $\psi^{(0)}$ and $T^{(0)}$ are:

$$t_e = \left(\frac{x}{\pi}\right)^2 \quad \text{for} \quad T^{(0)}$$

$$t_e = \frac{1}{\sigma}\left(\frac{x}{\beta_1}\right)^2 \quad \text{for} \quad \psi^{(0)}. \quad (32)$$

For $T^{(0)}$, the e-folding time is indicative of how long it takes for heat to be diffused across the local depth and, for $\psi^{(0)}$, it is the time taken for viscosity to diffuse momentum over the local depth. The important point here is that the e-folding times both vanish as x becomes small. That is, for any $t > 0$, there will be a region near the tip that will be exhibiting the large time behavior. Thus, even though the primary interest here is in the transient response, the 'large time' behavior will always be present somewhere in the flow domain.

4.2. *Temperature structure*

The asymptotic solution for $T^{(0)}$ [equation (26)] has three identifiable components. The first is a linear function of t which is independent of z. This term is the vertically averaged temperature. The second component is independent of t but is a function of z. This component is that part of the solution that balances the internal source and satisfies the flux boundary conditions. Lastly, there is the infinite sum of the transient terms that reflect the way the system approaches quasi-steady large time behavior. These terms ensure that the initial condition is satisfied.

Each of the components mentioned above has a different importance at different times and places. To see this, consider the case where x is fixed but arbitrary and allow t to increase from zero. The e-folding time of the transient terms increases with x. The initial transient phase persists until the vertical fluxes in the temperature profile are in equilibrium. When this occurs, there will be no change in the shape of the temperature profiles and the only time dependence will be a linear increase in the mean temperature. Which of the remaining two terms will dominate just after the transient terms have become negligible depends on x. Interestingly, there are three regimes; one near the tip where the t/x term is most important, one for moderate x where the vertical dependence is the most important and another for large x where the t/x term again dominates the behavior.

As $x \to 0$, that part of the solution that is z dependent remains finite while the t/x term increases without limit. Thus, there will be some region near $x = 0$ where t/x will dominate the behavior immediately after the transient terms have become negligible. Note that, as soon as the t/x term dominates, it will always dominate since it is the only term that increases with t.

As x becomes larger, the magnitude of the t/x term decreases but the z dependent term remains approximately constant (there are terms which are independent of x). This will lead to a region where the z dependent, t independent terms will dominate the temperature behavior immediately after the transient terms have vanished. In this region, the slope of the isotherms will be somewhere between vertical and horizontal reflecting the strong vertical dependence. Finally, as $x \to \infty$, the e-folding time of the transient terms increases with x^2 while the time taken for the t/x term to become important is linear with x. Thus, even though the z dependent, t independent terms do not vanish as $x \to \infty$: by the time that the transient terms have become negligible, the t/x term has already started to dominate the temperature structure. In other words, for very large x, the initial transient phase lasts longer than the time it takes for the t/x term to dominate the behavior of the temperature. This means that the vertical temperature structure is still evolving as the horizontal gradient associated with the t/x term dominates the overall structure.

Figure 2 shows a number of temperature profiles at $x = 1$ for times that include the initial regime where the structure is undergoing significant changes. For this value of x, the heating from the bottom boundary is more significant than that from internal heating. From $t = 0$ to $t = 0.03$, the heat that has been pumped in from the bottom boundary has diffused out into the core of the fluid. By $t = 0.04$, the profile has settled down to its large time behavior and the only significant change with time is an increase in the mean temperature associated with the linear time dependence. This figure provides an example of a region where the z-dependent terms dominate the behavior immediately after the transient terms have become small. Even though the transient terms are negligible for $t > 0.03$, the difference in the surface and bottom temperatures is larger than the mean temperature. This will be the case until the mean temperature has increased to a value larger than the temperature difference over the depth, which will occur at $t \approx 0.2$. Note that, in all of these profiles, there is warm, less dense fluid underlying cooler denser fluid. This is a potentially unstable situation. The issue of the stability of the $O(A^0)$ solutions found in this paper has been addressed by Farrow and Patterson [17].

Figure 3 shows the series of profiles of $T^{(0)}$ for the larger value of $x = 5$ at the same times as those of Fig. 2. At this value of x, the e-folding time is much larger and so it takes much longer for the profiles to reach their large time behavior. Note also that, for this value of x, the internal heating component dominates the bottom boundary heating and in fact the bottom is effectively insulated. The temperature structure at $x = 5$ will reach its large time behavior when the heat added near the surface has had time to diffuse to the bottom. This will occur at $t \approx 1$ which is greater than the time for the t/x term to become dominant. Thus, the t/x term will dominate the behavior before the shape of the temperature profile has stopped undergoing significant changes. Hence these profiles provide an example of the large x behavior discussed previously.

The overall structure of the temperature can be seen in Fig. 4 where temperature contours at $t = 0.5$ are shown. For $x < 0.5$, the isotherms are nearly vertical, indicating that the temperature there has reached its large time behavior. The temperature for $x < 0.5$ is given approximately by $T^{(0)} \approx t/x$. For $x > 3$, the bottom boundary is essentially insulated. Thus, at this time, the structure is divided into two regions; one with large horizontal temperature gradients and small vertical gradients and one with small horizontal temperature gradients and large vertical temperature gradients.

The development of the temperature structure with time can be seen in Fig. 5 where temperature contours are shown at $t = 5$. At this time, much of the plotted domain is showing the large time behavior with most of the isotherms being vertical. Thus, as time moves on, the point that divides the region with vertical isotherms from the region with horizontal isotherms moves out from $x = 0$. This occurs because the mean horizontal temperature gradient steadily increases

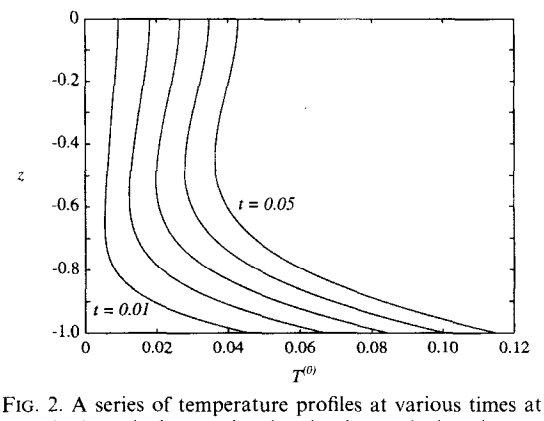

FIG. 2. A series of temperature profiles at various times at $x = 1$ where the bottom heating dominates the heat input.

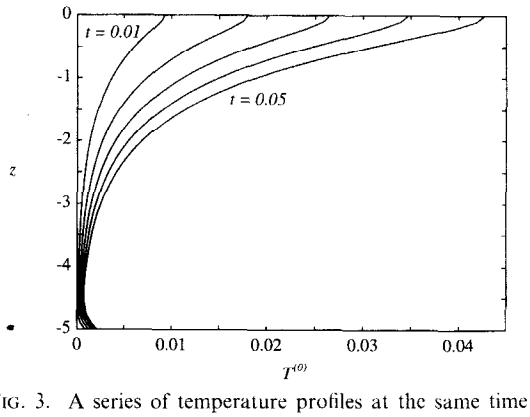

FIG. 3. A series of temperature profiles at the same time as the previous figure except at $x = 5$ where the internal absorption of radiation dominates the heat input.

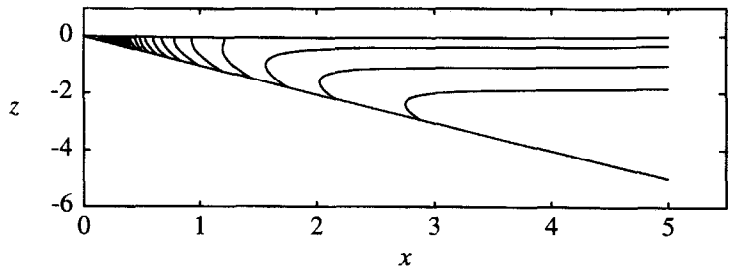

FIG. 4. Temperature contours at $t = 0.01$ showing the two regions with vertical and near horizontal isotherms.

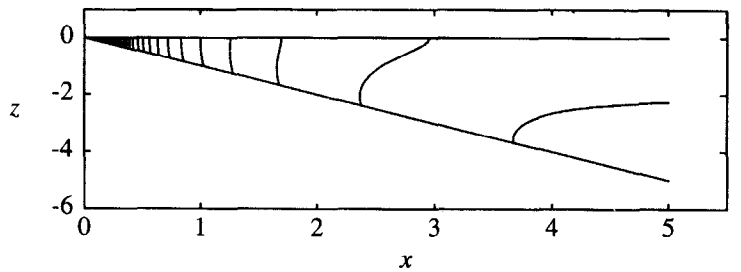

FIG. 5. Temperature contours at $t = 5.0$ showing how the structure has changed as more of the domain contains vertical isotherms.

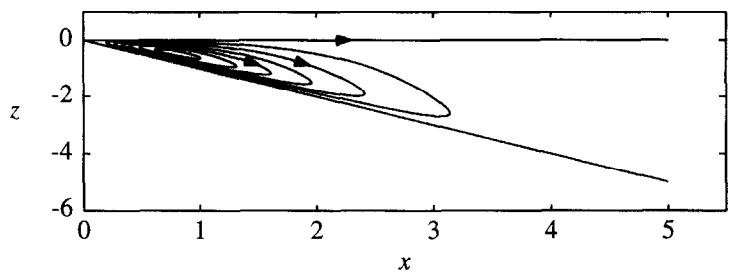

FIG. 6. Contours of $\psi^{(0)}$ at $t = 0.01$ showing the closed streamlines.

while the vertical gradient associated with the bottom and internal heating remains constant.

To summarize, the temperature response is characterized by three different regions; one with vertical isotherms near the tip, one with horizontal isotherms away from the tip and an intermediate section between these two regions which moves out from the tip as time progresses, reflecting the large time behavior influencing more and more of the temperature structure. Note that, in the horizontal isotherms region, the isotherms have to curl over to meet the bottom boundary condition at $z = -x$. As will be discussed later, this leads to a flow up the bottom boundary due to a mechanism described by Phillips [18] and Wunsch [19].

4.3. *Velocity field*

Much of the discussion about the way the temperature structure develops with time carries over to the velocity behavior. In particular, there is always some region near the tip that is exhibiting large time behavior and the size of this region increases with time. Figures 6 and 7 show two streamline plots at different times illustrating this. For $t = 0.01$ (Fig. 6) and $x < 0.5$, the streamfunction is well approximated by equation (31). However for $t = 5.0$ (Fig. 7), the large time behavior has occupied up to $x = 3$. As well as the size of the large time behavior region increasing with time, the magnitude of the circulation also increases with time. An important feature of both these figures is that all the streamlines are closed. This is quite different to the large time behavior given by equation (31). In fact, putting $z = -x/2$ into equation (31) shows that, at large times, $\psi^{(0)}$ is monotonically increasing in magnitude without limit as $x \to \infty$. The closed streamlines patterns can be explained in the following way. For any particular time, the temperature structure within the sidearm can be divided into two regions, one with vertical isotherms and one with horizontal isotherms. In the region with vertical isotherms, there is clearly a horizontal gradient that will drive a clockwise circulation. In the other region, the horizontal isotherms impose no horizontal pressure gradient and will thus not drive any flow. However, even in the latter region, the isotherms have to curl over to meet the bottom boundary condition. This curling over of the isotherms near $z = -x$ will, as pointed out by Phillips [18], lead to an upslope flow.

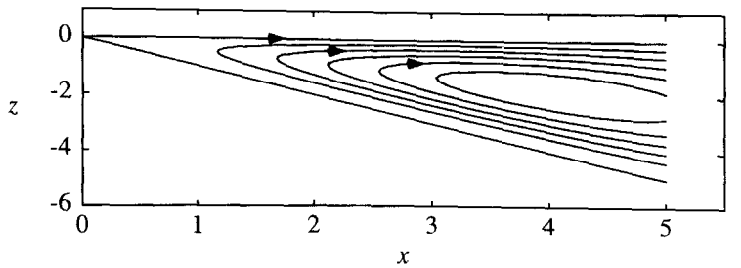

FIG. 7. Contours of $\psi^{(0)}$ at $t = 5.0$ showing how the flow develops with time with more of the domain demonstrating the large time behavior.

Phillips showed that the magnitude of the velocity up the slope was proportional to the background density gradient. In this case where the background density is a consequence of the internal heating, the gradient near the boundary dies off exponentially with x. This means that the magnitude of the upslope velocity will decrease exponentially with distance from the tip. This in turn leads to an exponential decrease of $\psi^{(0)}$ with x leading to the closed streamlines in Figs 6 and 7.

A clearer picture of the evolving flow can be seen in Fig. 8 where a series of velocity profiles at various times are plotted at $x = 2.5$. At $t = 0.02$, the flow due to the Phillips mechanisms can be seen clearly as a local upslope flow near the bottom $z = -2.5$. At this time and above $z = -2$, the velocity essentially has a plug profile, that is, the velocity is constant with depth. As time moves on, a number of things happen. Firstly, the flow up the slope accelerates. The flow near the bottom boundary is dominated by viscosity and thus the flow increases as the temperature gradient increases. At the same time, the slight background temperature gradient arising from the t/x term of $T^{(0)}$ is accelerating the core flow where a buoyancy–inertia balance holds. This leads to a linear velocity profile applying at the mid depths where the horizontal gradient due to this term is most dominant. This can be seen between $-2 < z < -1.5$ at $t = 0.12$. The e-folding time of the transient terms of the velocity at this value of x is much longer than $t = 0.12$, meaning that the flow is still inertial. The flow will remain inertial until it has accelerated to the point where vertical shear becomes important over the whole depth. When that time has been reached, the flow will be well approximated by the large time response in equation (31). Note also that as time increases the thickness of the upslope flow increases as viscosity diffuses momentum away from the boundary.

Figure 9 shows a series of velocity profiles at the same times as Fig. 8 except for a smaller value of $x = 0.25$. Here, the times are comparable to the e-folding time of the transient terms and so the flow becomes rapidly viscous. The transient terms of $T^{(0)}$ also vanish quickly here. The velocity profile rapidly becomes cubic and, by $t = 0.12$, is well approximated by the large time behavior (dashed line). Notice, however, that the full solution gives rise to larger velocities. This is because the other non-transient terms of $T^{(0)}$ and $\psi^{(0)}$ should be included as they will have a noticeable effect on the profile. The extra terms increase the temperature gradient there and will thus lead to an increased velocity.

One of the aims of this paper is to determine what effect a significant vertical density structure would have on the flow. This effect can now be deduced from the asymptotic solutions found above. When there is a significant vertical density structure, the most significant driving force for initiating a circulation in the sidearm is near the bottom boundary. The flow near the bottom boundary is driven either by the buoyancy

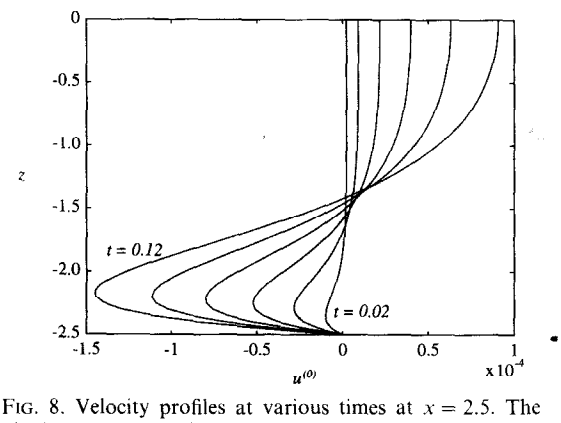

FIG. 8. Velocity profiles at various times at $x = 2.5$. The Phillips mechanism is generating an upslope flow evident near the bottom boundary.

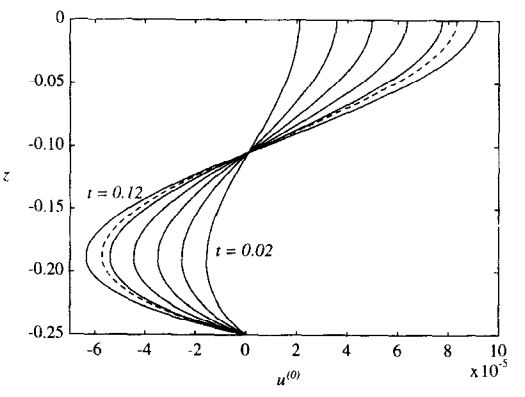

FIG. 9. Velocity profiles at $x = 0.25$ for the same time as the previous figure showing the rapid approach to viscous dominance. The dashed line is the large time behavior given by equation (31).

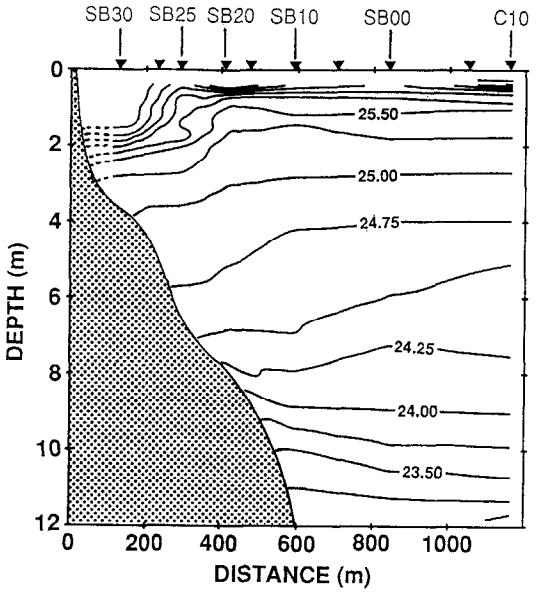

FIG. 10. Temperature contours in Salmon Brook at 12 noon in February (from Monismith *et al.* [3]).

flux associated with the temperature boundary condition there ($x < 1$) or the turning over of the isotherms to meet the effectively insulated bottom boundary condition ($x > 1$). In both cases, the stably stratified regions away from the bottom boundary are quite passive and the horizontal velocity in them is vertically constant and its magnitude is a result of conservation of mass; the flow up the slope must be balanced by a corresponding flow out away from the tip. The effect of the vertical stratification is limited to times less than the time it takes for viscosity to diffuse momentum over the local depth. For later times, the flow takes on the classic cubic profile of Cormack *et al.* [16]. Perhaps the most important effect of the vertical stratification is that it locks up energy that could otherwise be used to drive a stronger circulation. If the heat had been vertically averaged as it was in the model considered by Farrow and Patterson [13] for the diurnally forced case, the velocities would be larger. Thus, the strong stratification present during the day limits the magnitude of the circulation not because it retards motion but because it prevents the available energy from driving a stronger circulation; the energy has gone into vertical rather than horizontal gradients.

4.4. *Comparison with field observations*

There is some evidence that temperature structures similar to those just described occur in the field. Figure 10 shows temperature contours taken in Salmon Brook (a sidearm of Wellington Reservoir in Western Australia) at 12 noon in February [3]. For distances greater than 200 m from the tip, there is a strong vertical stratification associated with the absorption of solar radiation. For distances less than 200 m, however, there is a strong horizontal gradient. A more quantitative comparison between $T^{(0)}$ and field measurements is difficult since the real sidearm, unlike the idealized model, still has some structure associated with the previous night's cooling and other effects, such as wind, which are not included in the model considered in this paper.

The above asymptotic solutions can be used to estimate the magnitude of the daytime velocity in a real sidearm. For the sidearm considered by Monismith *et al.* [3], the bulk parameters are $A \approx 0.02$ and $I_0 \approx 300$ W m^{-2}. There is no indication from Monismith *et al.* about appropriate values for η: however, from Kirk [2], a representative value is $\eta \approx 2$ m^{-1}. During the day, the velocities in a sidearm are typically small and there is a strong, stable stratification suggesting that molecular values are appropriate for ν and κ. Assuming that the heating has been underway for 6 h, which corresponds to a non-dimensional time of $t = 0.01$, and the usual values for the remaining parameters, the model described above yields a maximum horizontal velocity of 10 cm s^{-1}. This is consistent with the observations of Monismith *et al.* [3] and Adams and Wells [4] where maximum velocities of 7.5–15 cm s^{-1} were reported. The value of 10 cm s^{-1} should be contrasted with that of 90 cm s^{-1} that would arise if the heat had been uniformly distributed in the vertical [13] and so the more realistic modelling of the heat input has had a significant effect on the results of this model.

5. CONCLUDING REMARKS

This paper has addressed the effect that vertical stratification has on the flow in a reservoir sidearm. This is particularly important during the day where the absorption of solar radiation leads to a strong vertical temperature gradient, especially near the surface. The model formulated to examine this led to a temperature field that reflected observed daytime temperature structures in real sidearms. The sidearm can be divided into two main regions; one with vertical isotherms and one with horizontal isotherms. In the former region, horizontal gradients are large and drive a circulation with a surface outflow. In the latter region, the horizontal isotherms must curl over to meet the flux boundary condition at the sloping bottom. This leads to an upslope flow due to a mechanism described by Phillips [18]. The magnitude of the upslope flow is proportional to the strength of the vertical density gradient in the vicinity of the bottom boundary. This strength decreases exponentially with distance from the tip leading to closed streamlines. This is different to what would occur if the heat had been distributed uniformly in the vertical. Thus, the primary effect of the vertical stratification is to change

the geometry of the flow such that the flow is restricted to a region near the tip whose size increases with t.

Acknowledgements—The authors are grateful to Steven Armfield and John Taylor for valuable comments on earlier drafts of this paper. The research described in this paper was carried out while one of us (DF) was a recipient of an Australian Postgraduate Research Award along with a Centre for Water Research Scholarship.

REFERENCES

1. J. Imberger and J. C. Patterson, Physical limnology, *Adv. Appl. Mech.* **27,** 303–475 (1990).
2. J. T. O. Kirk, Optical limnology—a manifesto. In *Limnology in Australia* (Edited by P. de Dekker and W. D. Williams), pp. 33–62 (1986).
3. S. G. Monismith, J. Imberger and M. L. Morison, Convective motions in the sidearm of a small reservoir, *Limnol. Oceanogr.* **35,** 1676–1702 (1990).
4. E. E. Adams and S. A. Wells, Field measurements on side arms of Lake Anna, Va, *J. Hyd. Eng.* **110,** 773–793 (1984).
5. T. W. Sturm, Laminar convection of heat in dead-end channels, *J. Fluid Mech.* **110,** 99–114 (1981).
6. S. C. Jain, Buoyancy-driven circulation in free-surface channels, *J. Fluid Mech.* **112,** 1–12 (1982).
7. D. N. Brocard and D. R. F. Harleman, Two-layer model for shallow convective circulation, *J. Fluid Mech.* **100,** 129–156 (1980).
8. D. Poulikakos and A. Bejan, The fluid mechanics of an attic space, *J. Fluid Mech.* **131,** 251–269 (1983).
9. C. F. Scott and J. Imberger, Three-dimensional estuary circulation and classification. *Proceedings of International Conference on Physics of Shallow Estuaries and Bays* (1988).
10. C. F. Scott, On the circulation and classification of shallow estuaries, Ph.D. Thesis, University of Western Australia (1988).
11. J. C. Patterson, Unsteady natural convection in a cavity with internal heating, *J. Fluid Mech.* **140,** 135–151 (1984).
12. J. C. Patterson, A model for convective motions in reservoir sidearms. *Proceedings XXII Congress IAHR, Lausanne*, pp. 68–73 (1987).
13. D. E. Farrow and J. C. Patterson, On the response of a reservoir sidearm to diurnal heating and cooling. *J. Fluid Mech.* **246,** 143–161 (1993).
14. A. Rabl and C. Nielson, Solar ponds for space heating, *Sol. Energy* **17,** 1–12 (1975).
15. D. E. Cormack, L. G. Leal and J. Imberger, Natural convection in a shallow cavity with differentially heated end walls. Part 1. Asymptotic theory, *J. Fluid Mech.* **65,** 209–229 (1974).
16. D. E. Cormack, G. P. Stone and L. G. Leal, The effect of upper surface conditions on convection in a shallow cavity with differentially heated end-walls. *Int. J. Heat Mass Transfer* **18,** 635–648 (1975).
17. D. E. Farrow and J. C. Patterson, On the stability of the near shore waters of a lake when subject to solar heating, *Int. J. Heat Mass Transfer* **36,** 89–100 (1993).
18. O. M. Phillips, On flows induced in a stably stratified fluid, *Deep Sea Res.* **17,** 435–443 (1970).
19. C. Wunsch, On oceanic boundary mixing, *Deep Sea Res.* **17,** 293–301 (1970).

APPENDIX A

The functions $\psi_1^{(0)}$, $\psi_2^{(0)}$, $\psi_3^{(0)}$, $\psi_{4n}^{(0)}$, $\psi_{5n}^{(0)}$, and $\psi_{6n}^{(0)}$ are given by:

$$\psi_1^{(0)} = \frac{1}{48\sigma} z(z+x)^2(2z-x) - \frac{2x^3}{\sigma} \sum_{n=1}^{\infty} \frac{1}{\beta_n^4 \sin \beta_n} \{[x \sin(\beta_n z/x) - z \sin \beta_n] \times [\cos \beta_n + (\cos \beta_n - 1)/\beta_n^2 - \tfrac{1}{2}] \exp[-\sigma(\beta_n/x)^2 t]\}, \tag{A1}$$

$$\psi_2^{(0)} = \frac{1}{720\sigma} z(z+x)^2(2z^3 - 4xz^2 + 6x^2 z - 3x^3) + \frac{2x^5}{\sigma} \sum_{n=1}^{\infty} \frac{1}{\beta_n^6 \sin \beta_n} \{[x \sin(\beta_n z/x) - z \sin \beta_n] \times [1 - \beta_n^2/4 - 2\cos \beta_n - 2(\cos \beta_n - 1)/\beta_n^2] \times \exp[-\sigma(\beta_n/x)^2 t]\}, \tag{A2}$$

$$\psi_3^{(0)} = \frac{t}{48\sigma} z(z+x)^2(2z-x) + \frac{2x^5}{\sigma^2} \sum_{n=1}^{\infty} \frac{1}{\beta_n^6 \sin \beta_n} \{[x \sin(\beta_n z/x) - z \sin \beta_n] \times [\cos \beta_n + (\cos \beta_n - 1)/\beta_n^2 - \tfrac{1}{2}](1 - \exp[-\sigma(\beta_n/x)^2 t])\}. \tag{A3}$$

The remaining solutions $\psi_{4n}^{(0)}$, $\psi_{5n}^{(0)}$ and $\psi_{6n}^{(0)}$ can all be written in the following way:

$$\psi_{kn}^{(0)} = \frac{\sin\left(\frac{n\pi z}{x\sqrt{\sigma}}\right) - \frac{n\pi z}{x\sqrt{\sigma}} \cos\left(\frac{n\pi z}{x\sqrt{\sigma}}\right)}{\sin(n\pi/\sqrt{\sigma}) - (n\pi/\sqrt{\sigma}) \cos(n\pi/\sqrt{\sigma})} F_{kn0}|_{z=-x} + \frac{x \sin\left(\frac{n\pi z}{x\sqrt{\sigma}}\right) - z \cos\left(\frac{n\pi}{\sqrt{\sigma}}\right)}{\sin(n\pi/\sqrt{\sigma} - (n\pi/\sqrt{\sigma}) \cos(n\pi\sqrt{\sigma})} \left.\frac{\partial F_{kn0}}{\partial z}\right|_{z=-x} + F_{kn0}(x,z,t) - \frac{2\sigma}{x^3} \sum_{m=1}^{\infty} \frac{1}{\sin \beta_n} \times [x \sin(\beta_m z/x) - z \sin \beta_m] \left(F_{knm}|_{z=-x} + x \left.\frac{\partial F_{knm}}{\partial z}\right|_{z=-x} \right), \tag{A4}$$

where $k = 4$, 5 and 6, $n = 1, 2, \ldots$ and the functions F_{knm} are given below:

$$F_{4n0} = -\frac{1}{\sigma - 1} \left(\frac{x}{n\pi}\right)^4 \left\{ [\cos(n\pi z/x) - 1] - \sigma \left[\cos\left(\frac{n\pi z}{x\sqrt{\sigma}}\right) - 1 \right] \right\} \exp[-(n\pi/x)^2 t], \tag{A5}$$

$$F_{4nm} = \frac{x^4}{\sigma} \left(\frac{x}{n\pi}\right)^2 \frac{1}{(n\pi)^2 - \beta_m^2} \frac{1}{(n\pi)^2 - \sigma/\beta_m^2} \{[\cos(n\pi z/x) - 1] - (n\pi/\beta_m)^2 [\cos(\beta_m z/x) - 1]\} \exp[-\sigma(\beta_m/x)^2 t], \tag{A6}$$

$$F_{5n0} = -\frac{1}{\sigma - 1} \left(\frac{x}{n\pi}\right)^4 \left\{ [\cos(n\pi z/x) - 1] - \sigma \left[\cos\left(\frac{n\pi z}{x\sqrt{\sigma}}\right) - 1 \right] \right\} t \exp[-(n\pi/x)^2 t], \tag{A7}$$

$$F_{5nm} = \frac{x^6}{\sigma} \left(\frac{x}{n\pi}\right)^2 \frac{1}{(n\pi)^2 - \beta_m^2} \frac{1}{[(n\pi)^2 - \sigma/\beta_m^2]^2} \times \{[\cos(n\pi z/x) - 1] - (n\pi/\beta_m)^2 [\cos(\beta_m z/x) - 1]\} \times \{\exp[-\sigma(\beta_m/x)^2 t] - \exp[-(\beta_m/x)^2 t]\}, \tag{A8}$$

$$F_{6n0} = -\frac{1}{1-\sigma}\left(\frac{x}{n\pi}\right)^4 \left\{\frac{2x}{n\pi}\frac{2\sigma-1}{\sigma-1}[\cos(n\pi z/x)-1]\right.$$
$$+ z\sin(n\pi z/x) - \frac{2\sigma^2}{\sigma-1}\frac{x}{n\pi}$$
$$\left.\times\left[\cos\left(\frac{n\pi z}{x\sqrt{\sigma}}\right)-1\right]\right\}\exp[-(n\pi/x)^2 t], \quad \text{(A9)}$$

$$F_{6nm} = -\frac{x^4}{\sigma}\left(\frac{x}{n\pi}\right)\frac{1}{(n\pi)^2-\beta_m^2}\frac{1}{(n\pi)^2-\sigma\beta_m^2}$$
$$\times\left\{\frac{2x}{n\pi}\frac{2(n\pi)^2-\beta_m^2}{(n\pi)^2-\beta_m^2}[\cos(n\pi z/x)-1]\right.$$
$$+ z\sin(n\pi z/x) - \frac{2x^4}{\beta_m^2}\left(\frac{n\pi}{x}\right)^3\frac{1}{(n\pi)^2-\beta_m^2}$$
$$\left.\times[\cos(\beta_m z/x)-1]\right\}\exp[-\sigma(\beta_m/x)^2 t], \quad \text{(A10)}$$

where in the above equations β_m, $m = 1, 2, \ldots$, are the positive roots of the equation $\sin\beta_m = \beta_m\cos\beta_m$.